Weak exchange striction between the 4*f* and 3*d* ions in the multiferroic $GdMn_2O_5$

Jieming Sheng,[1,2] X. Tong,[3] Feng Ye,[2,*] J. A. Fernandez-Baca,[2] H. Cao,[2] N. Poudel,[4] M. Gooch,[4] B. Lorenz,[4] C. W. Chu,[4] Xueyun Wang,[5] and S.-W. Cheong[5]

[1]*Department of Physics, Renmin University of China, Beijing 100872, China*

[2]*Neutron Scattering Division, Oak Ridge National Laboratory, Oak Ridge, Tennessee 37831, USA*

[3]*Neutron Technologies Division, Oak Ridge National Laboratory, Oak Ridge, Tennessee 37831, USA*

[4]*Texas Center for Superconductivity and Department of Physics, University of Houston, Houston, Texas 77204, USA*

[5]*Rutgers Center for Emergent Materials and Department of Physics and Astronomy, Rutgers University, Piscataway, New Jersey 08854, USA*

(Received 15 November 2018; published 21 March 2019)

We used single-crystal neutron diffraction to investigate the magnetic structures of the multiferroic $GdMn_2O_5$. The system undergoes a first-order incommensurate to commensurate magnetic transition below 33 K, accompanied by the appearance of electric polarization *P*. Upon cooling, *P* increases smoothly while the magnetic order shows an abrupt enhancement in intensity below 20 K owing to the large increase of the rare-earth Gd moment. The contrasting temperature evolution of the magnetic order and polarization indicates the polarization is mainly driven by the exchange striction between the magnetic Mn ions. The incommensurate phase in the intermediate temperature range has a cycloidal modulation along the *c* axis, with spin configuration projected in the *ab* plane similar to the commensurate phase. The lack of observable bulk polarization suggests the exchange striction is not the dominant mechanism for the polarization in the incommensurate phase.

DOI: 10.1103/PhysRevB.99.094429

The RMn_2O_5 manganites, where *R* is a rare earth, Y, or Bi, have drawn considerable attention due to the ferroelectricity induced by magnetism and the large magnetoelectric coupling [1–6]. The family has an orthorhombic structure with the centrosymmetric *Pbam* space group at room temperature, and consists of edge-shared $Mn^{4+}O_6$ octahedral chains along the *c* axis and pairs of $Mn^{3+}O_5$ pyramids connecting the octahedral chains [7]. Due to the strong spin frustration arising from the competing exchange interactions between Mn^{3+} and Mn^{4+}, RMn_2O_5 exhibits noncollinear antiferromagnetic (AFM) structures and complex magnetic phases [8]. The system typically has successive magnetic phase transitions within a narrow range of temperature (*T*) below 45 K, accompanied by the variation of ferroelectric polarization [9–11]. Because of the nearly collinear magnetic structure [6], the ferroelectricity is presumably driven by the symmetric exchange-striction mechanism [12,13]. The exchange interaction between the neighboring Mn spins $\vec{S}_i$ and $\vec{S}_j$ induces collective displacements along the *b* axis and leads to polarization $P \propto \prod_{ij}(\vec{S}_i \cdot \vec{S}_j)$. The polarization of RMn_2O_5 is generally of moderate size, ranging from a few hundreds to thousands of $\mu C/m^2$ [14]. Among the family, $GdMn_2O_5$ (GMO) exhibits exceptional properties of larger polarization (3600 $\mu C/m^2$) and giant tunability of the polarization under magnetic field [9]. It was initially attributed to the strong exchange interaction between the rare-earth Gd and the transition metal Mn ions, where the Gd moments align nearly parallel with the neighboring Mn^{3+} ions [9]. However, this scenario remains controversial since a similar feature is not observed in the isostructural members RMn_2O_5 (R = Tb, Ho, and Dy) with commensurate (CM) order [2–4,10,15]. Therefore, a detailed characterization of the magnetic structures is necessary to understand the microscopic mechanism for the ferroelectricity.

In this paper, we present a comprehensive single-crystal neutron-diffraction study of the magnetic structures in GMO. The low-*T* AFM structure is nearly collinear with CM wave vector (1/2, 0, 0). The Gd and Mn spins form AFM zigzag chains in the *ab* plane and ferromagnetic (FM) stacking along the *c* axis. Although the electric polarization shows a smooth increase upon cooling, the intensity of characteristic magnetic Bragg peaks exhibits an abrupt increase below 20 K. Magnetic structure refinements reveal that the anomalous behavior of the magnetic order parameter is due to the drastic enhancement of the ordered Gd moments. Our results indicate that the exchange striction between 4*f*-3*d* moments is weak, and the polarization is mainly driven by the Mn^{4+}-Mn^{3+} interactions. As the system is warmed above 33 K in the incommensurate (ICM) phase, the magnetic configuration evolves into a cycloidal modulation with moments mainly lying in the *ab* plane. The absence of *P* indicates the exchange striction is not the dominant mechanism for the polarization in the ICM phase.

Single crystals of GMO were grown using a B_2O_3-PbO-PbF_2 flux in a Pt crucible [3] with typical size of $1 \times 1 \times 0.5$ mm^3. Isotopic Gd ($Z = 158$) is used to alleviate the severe absorption in the neutron-diffraction study. The experiments are carried out using the four-circle single-crystal diffractometer HB3A [16] at the High Flux Isotope Reactor with incident wavelength 1.5424 Å, and the single-crystal diffuse scattering spectrometer CORELLI at the Spallation Neutron Source [17]. A closed-cycle refrigerator is used to regulate the temperature of the sample.

*yef1@ornl.gov

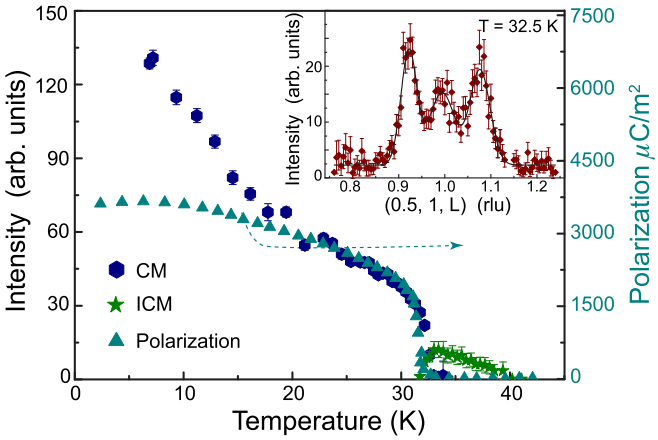

FIG. 1. The T dependence of the CM and ICM magnetic Bragg reflections $(1/2, 1, 1)$ and $(1/2, 1, 1+\delta)$, as well as the ferroelectric polarization reported in $GdMn_2O_5$ [9]. The inset shows the wave-vector scan at 32.5 K across the magnetic peak $(1/2, 1, 1)$ revealing the coexisting CM and ICM components.

Figure 1 displays the T dependence of the magnetic reflection $(1/2, 1, 1)$ and the corresponding phase transitions in GMO. The sample enters an ICM spin configuration at $T_{N1} \sim 40$ K, with magnetic propagation wave vector characterized as $q_{\mathrm{ICM}} = (1/2, 0, \delta)$. The intensity of the ICM Bragg peak increases upon cooling, and experiences a suppression at $T_{N2} \approx 33$ K. Another magnetic order with a CM wave vector $q_{\mathrm{CM}} = (1/2, 0, 0)$ emerges along with the simultaneous occurrence of the electric polarization. The coexisting CM and ICM phases in a small temperature window (inset of Fig. 1) suggest the transition is of first order, which is commonly observed in other RMn_2O_5 [18,19].

The CM magnetic structure of GMO was studied using synchrotron x-ray magnetic scattering and neutron powder diffraction [9,21]. It is described as an AFM order with wave vector $(1/2, 0, 0)$. The corresponding magnetic space group (MSG) is P_aca2_1, which is one of the two allowed irreducible representations with order parameter in the direction $(a, 0)$. In the magnetic x-ray measurement, the spin direction of the Gd ions is determined through azimuthal scans to be approximately along the a axis. However, the moment size and spin direction of Mn ions are not characterized, which prevents an accurate assessment of the underlying mechanism for the induced polarization. The relatively simple form of the magnetic cross section in neutron scattering can provide straightforward and detailed information of the magnetic structure. We carried out single-crystal neutron-diffraction measurement at different temperatures at the HB3A four-circle single-crystal diffractometer. The magnetic structure is analyzed based on the paramagnetic crystal structure space group $Pbam$ and the wave vector $(1/2, 0, 0)$ [22–25]. Four maximal magnetic space groups with nonzero magnetic moments, P_aca2_1 (No. 29.104), P_bmc2_1 (No. 26.72), P_c2/c (No. 13.72), and P_a2/m (No. 10.47) are possible, where the number inside the parentheses is the Belov-Neronova-Smirnova notation of the magnetic space group. The initial spin configuration is tested using the simulated annealing method [26]. Further refinement indicates that the MSG P_aca2_1 is the correct one to describe the intensities of observed magnetic reflections. Since there are 12 magnetic ions in the chemical unit cell, 36 spin degrees of freedom in total need to be determined. The magnetic symmetry analysis greatly reduces the number of refinable parameters. For the MSG P_aca2_1, the Gd^{3+} and Mn^{3+} ions are split into two independent sites due to the loss of the inversion center, and the spin moments are free to rotate in the ab plane. The Mn^{4+} site remains unsplit with moment direction allowed along all crystallographic axes. Thus, only 11 spin components (4 for Gd and 7 for Mn ions) need to be refined. We have collected about 70 independent magnetic reflections which are sufficient to quantify the spin components of an individual site. The refined parameters are summarized in Table I of the Appendix. The spin configurations at 5 and 20 K are overall similar. One of the key differences is the z component of Mn^{4+} is reduced indicating its moment is more coplanar with neighboring Mn^{3+} ions; the other feature is that the ordered moment for Gd^{3+} increases nearly twofold compared to the value at 20 K. The symmetry operators of the MSG P_aca2_1 [with coordinates defined in $(a_p, c_p, -b_p)$, where a_p, b_p, and c_p are the parent $Pbam$ basis] without time reversal constitute a polar space group $Pb2_1m$ in the parent setting. This naturally gives rise to the polarization along the b axis, consistent with the experimental observation. Consequently, there is a notable difference in refined magnetic moment size for the $Mn_1{}^{3+}$ and $Mn_2{}^{3+}$ spins caused by the split of the Mn^{3+} sites at both 5 and 20 K (Table I). The corresponding charge valences of the Mn_1^{3+} and Mn_2^{3+} spins are $+3.12(2)$ and $+3.00(2)$ as calculated using the bond valence summation method [27].

Figure 2 illustrates the spin structure at 5 K. The configuration is almost identical to the result by Lee *et al.* [9,25], but bears a subtle difference with the recent neutron powder diffraction report [21]. The Gd^{3+} and Mn^{3+} spins marked in Fig. 2 have FM coupling, instead of AFM correlation described in Ref. [21]. The latter configuration is simply the nontrivial magnetic domain with the 2_1-rotation axis applied instead of the mirror plane across $(1/4, 0, 0)$ in our case. Both spin configurations correctly describe the low-T magnetic scattering intensity except opposite polarizations. Like other RMn_2O_5 in their polar phases, the q_x component is locked at $1/2$ indicating the magnetic unit cell is doubled along the a axis [10,28]. In the ab plane, the Mn spins are arranged in a loop consisting of five Mn spins, Mn^{4+}-Mn^{3+}-Mn^{3+}-Mn^{4+}-Mn^{3+} (lower right corner of Fig. 2). The AFM nearest-neighbor coupling in the loop and the odd number of Mn-Mn bonds lead to spin frustration. This prevents the spins from being antiparallel on every bond and results in a noncollinear magnetic structure [12]. Along the zigzag chain in the b direction, the spins of the neighboring Mn^{3+} and Mn^{4+} are close to collinear. According to the exchange striction model, Mn^{3+} spins parallel to the Mn^{4+} (blue dashed circle) move closer to the Mn^{4+} (which is fixed at the special position), while Mn^{3+} spins with antiparallel configuration (red dashed circle) move away [9,13]. This mechanism leads to both the a- and b-axis displacements of the Mn^{3+} cations. Only the net polarization survives along the b axis as the one along the a axis cancels out.

The large polarization in GMO indicates that there might be an additional contribution other than the exchange striction

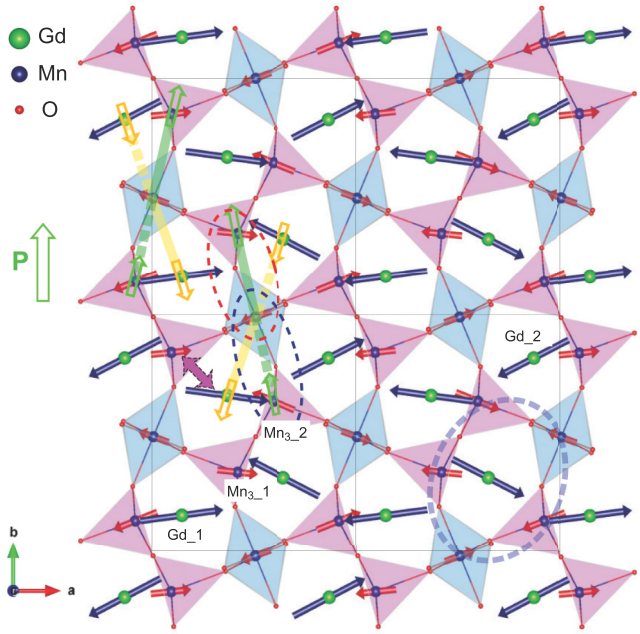

FIG. 2. The crystal and CM magnetic structures of GMO projected in the ab plane. The Mn^{4+} ions located at $(0, 0.5, 0.256)$ and Mn^{3+} ions at $(0.412, 0.352, 0.5)$ form (blue) MnO_6 octahedra and (pink) MnO_5 pyramids. The blue and red solid arrows represent the Gd and Mn spin moments. The dotted and solid lines (green and yellow) indicate attractive and repulsive interactions between the Mn^{3+}-Mn^{4+} and Gd^{3+}-Mn^{4+} pairs. The green (yellow) open arrows indicate the Mn^{3+} (Gd^{3+}) displacement. The large green arrow is the overall ionic displacements corresponding to a net macroscopic polarization. Note the FM couplings between the Mn^{3+} and Gd ions are marked by purple arrows (see main text). The structure is drawn using VESTA software [20].

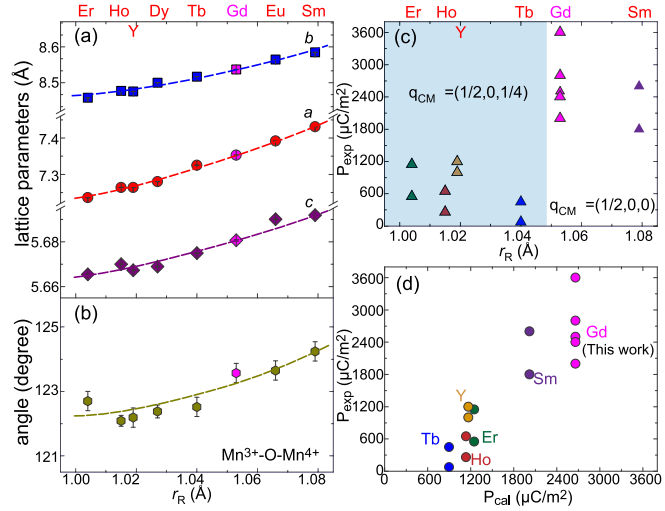

FIG. 3. (a) The lattice parameters of RMn_2O_5 as a function of radius r_R of the rare-earth element (data are from Refs. [7,33–35]). (b) The in-plane Mn^{3+}-O-Mn^{4+} bond angle versus r_R [36]. The data for GMO are from our single-crystal x-ray diffraction study. Curves are guides to the eye. (c) The measured polarizations as a function of r_R are from Refs. [2–4,9,14,37–45]. Data fluctuations are due to the reports from different groups. (d) The comparison of measured and calculated polarizations based on the second term of Eq. (1). The polarizations of the RMn_2O_5 compounds in their CM phase are calculated by considering only the magnetoelectric coupling constant c_2 of Mn^{3+}-Mn^{4+} and their magnetic structures reported in Refs. [6,10,41,46].

between the Mn^{3+}-Mn^{4+} ions. For example, the activation of Gd^{3+}-Mn^{4+} exchange could play a crucial role as suggested by distinct critical behavior in the resonant and nonresonant scattering [9]. Because of the quasicollinear spin arrangement, the polarization induced by the symmetric exchange striction model [29] should be much stronger than the antisymmetric Dzyaloshinskii-Moriya (DM) exchange interaction in the CM phase [30–32], and can be evaluated as

$$P_b \approx 2c_1\vec{M}^{\mathrm{Mn}^{4+}}[\vec{M}^{\mathrm{Gd}_2{}^{3+}}\cos\Phi_2 - \vec{M}^{\mathrm{Gd}_1{}^{3+}}\cos\Phi_1]\cos\Phi_3 + 2c_2\vec{M}^{\mathrm{Mn}^{4+}}[\vec{M}^{\mathrm{Mn}_2{}^{3+}}\cos\Phi_5 - \vec{M}^{\mathrm{Mn}_1{}^{3+}}\cos\Phi_4]\cos\Phi_3. \quad (1)$$

Here, c_1 and c_2 are the magnetoelectric coupling constants for the Gd^{3+}-Mn^{4+} and Mn^{3+}-Mn^{4+} pairs, and Φ_i is the phase for each magnetic site (details in the Appendix). The refined parameters of individual magnetic ions and the reported polarization [9] at 5 and 20 K allow quantitative evaluation of the Gd^{3+}-Mn^{4+} and Mn^{3+}-Mn^{4+} contribution separately. A ratio of $c_1/c_2 \simeq -1/6$ is obtained, and this implies the exchange striction between the Gd^{3+}-Mn^{4+} ions is considerably smaller than that between the Mn^{3+}-Mn^{4+} ions. Furthermore, the opposite signs of c_i indicate the atomic displacement caused by Gd^{3+} is canceling the contribution from the Mn^{3+}. Taken together, the magnetoelectric coupling between the 4f and 3d ions is not responsible for the large polarization in GMO. This conclusion is quite evident by comparing the T dependence of the polarization and magnetic order (Fig. 1). The polarization increases smoothly upon cooling, while the magnetic order displays a sharp increase below 20 K. The ordered Gd moments are almost doubled at base T while the Mn moments increase less than 20%. One would expect more enhanced polarization if the exchange striction between Gd-Mn moments is significant.

To understand whether there is a correlation between the polarization P and the structural properties, we plot in Figs. 3(a) and 3(b) the structural evolution with increasing rare-earth radius r_R. From the smallest Er to the largest Sm, both the lattice parameters and the in-plane Mn^{3+}-O-Mn^{4+} bond angle relevant for the b-axis polarization increase systematically and show no sign of anomaly across the series. However, the measured polarization $P_{\mathrm{expt.}}$ exhibits a notable trend with increasing r_R, as shown in Fig. 3(c). The RMn_2O_5 system can be classified into two groups, one with larger $P_{\mathrm{expt.}}$ and a characteristic wave vector of $(1/2, 0, 0)$, and the other with much smaller $P_{\mathrm{expt.}}$ and a wave vector of $(1/2, 0, 1/4)$. It is clear that bigger rare-earth ions promote FM exchange interaction between the Mn^{4+} and Mn^{4+} spins through the R layer [9]; this results in larger staggered moments on the Mn^{4+} sites. In contrast, the system with smaller r_R has a cycloidal spin modulation [6,10,47]. The presence of $q_z = 1/4$ not only enables a symmetry-allowed out-of-plane spin component, but also introduces an $\sim\pi/4$ and $\pi/8$ phase shift at the Mn^{3+} and Mn^{4+} sites, respectively, that effectively

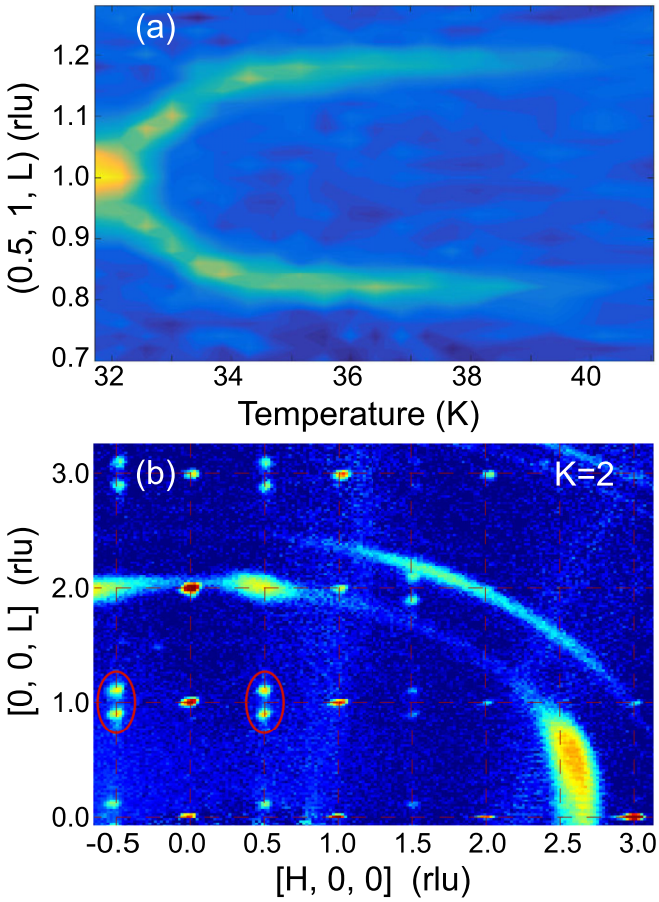

FIG. 4. (a) The evolution of ICM magnetic reflection $(1/2, 1, 1 \pm \delta)$ with increasing temperature. (b) The diffraction image in the $(h, k = 2, l)$ scattering plane at 33.5 K. The split ICM magnetic reflections in red circles have a propagation vector of $(1/2, 0, 0.1)$.

reduces the ordered moment. Furthermore, the reduced Mn^{3+}-O-Mn^{4+} bond angle with decreasing r_R weakens the AFM interaction [48]. All of the above factors contribute to a smaller polarization for the system with smaller r_R. As illustrated in Fig. 3(d), the calculated polarization based on the term involving only the exchange striction between the Mn ions describes qualitatively well the measured $P_{\text{expt.}}$ [49]. This confirms the polarization in $R\text{Mn}_2\text{O}_5$ is predominantly driven by the interactions between the $3d$ magnetic ions. On the other hand, the role of the magnetic rare-earth ions cannot be overlooked. For example, a large critical magnetic field of $H_C \approx 18$ T is needed to reverse the polarization in BiMn_2O_5 where the Bi element is nonmagnetic [5]. The critical fields are suppressed to 2 and 5 T for TbMn_2O_5 and GdMn_2O_5, respectively [2,9]. It is found that the moments of rare-earth ions are rather easy to rotate under a magnetic field [50]. Once polarized, they act cooperatively with the external field to drive a spin-flop transition that reverses the polarization at a lower critical field.

The ICM magnetic structure of GdMn_2O_5 for $T > 33$ K is studied using the CORELLI diffractometer. Figure 4(a) shows the evolution of the magnetic peak $(1/2, 1, 1 \pm \delta)$ with increasing temperature, where the ICM component of magnetic wave vector increases gradually to $\delta = 0.19$. The intensity of ICM magnetic order disappears at 40 K. Figure 4(b) shows the contour plot of the diffraction image in the $(h, k = 2, l)$ scattering plane at 33.5 K with only ICM peaks at $q_{\text{ICM}} = (1/2, 0, 0.1)$. The modulated spin structure is analyzed using the magnetic superspace symmetry formalism as it provides a robust treatment of the magnetic constraint [51]. In this approach, the spin component of each magnetic atom μ located at $\mathbf{r}_\mu$ inside the unit cell $\mathbf{l}$ is expressed as

$$\mathbf{M}_{\mu,\mathbf{l}}(x_4) = \mathbf{M}_\mu e^{-2\pi i x_4} + \mathbf{M}_\mu^* e^{2\pi i x_4}, \tag{2}$$

where $x_4 = \mathbf{k} \cdot (\mathbf{l} + \mathbf{r}_u)$ defines the internal coordinate of the modulated spin structure. The symmetry relation between the magnetic modulation functions of two atoms under a superspace symmetry operation $\{\mathbf{R}, \theta|\mathbf{t}, \tau\}$ is given by

$$\mathbf{M}_{\mu,\mathbf{l}}(R_I x_4 + \tau) = \theta \det(\mathbf{R}) \cdot \mathbf{M}_\nu(x_4), \tag{3}$$

where $\mathbf{R}$ is the point-group operation, θ being -1 or $+1$ depending on whether the operation includes time reversal or not, $\mathbf{t}$ is a translation in real space, and R_I is $+1$ or -1 if $\mathbf{R}$ keeps $\mathbf{k}$ invariant or transforms $\mathbf{k}$ into $-\mathbf{k}$. We use Jana2006 [52] to analyze the ICM magnetic structure of GMO. Out of the possible Shubnikov magnetic superspace groups (MSSG) of $Pb2_1m.1'(1/2, 0, g)$, $P2_1/a.1'(a, 0, g)$, and $P2/m.1'(1/2, 0, g)$, only the MSSG $Pb2_1m.1'(1/2, 0, g)$ best describes the ICM magnetic phase. It can be further simplified to $Xb2_1m.1'(0, 0, g)$ with a new magnetic wave vector $(0, 0, \delta)$ by introducing the appropriate centering translation in superspace, i.e., a magnetic cell that doubles along the a direction. The $(1/2, 0, 0)$ component of the original ICM wave vector means the atoms related by a translation a have modulation with a π phase shift. The individual symmetry operators of the MSSG provide stringent constraints of the magnetic components. For example, the mirror plane operation perpendicular to the c axis "m_c" keeps Mn^{3+} atoms invariant and therefore constrains the form of its modulation. According to Eq. (3),

$$\mathbf{M}_{\text{Mn}^{3+}}(-x_4 + 1/2) = m_c \cdot \mathbf{M}_{\text{Mn}^{3+}}(x_4). \tag{4}$$

Consider the spin components $M_x(x_4)$, $M_y(x_4)$, and $M_z(x_4)$ of the magnetic modulation function of Mn^{3+} along the three crystallographic directions; Eq. (4) implies the following relations:

$$\begin{aligned} M_x(-x_4 + 1/2) &= -M_x(x_4), \\ M_y(-x_4 + 1/2) &= -M_y(x_4), \\ M_z(-x_4 + 1/2) &= M_z(x_4). \end{aligned} \tag{5}$$

Equations (5) indicate that modulation of the x, y components of the Mn^{3+} moments should be cosinelike, and the z component should be sinelike. Thus the Mn^{3+} moments form a cycloid order with two principal axes lying within the ab plane and along the c axis, respectively. The same requirement applies to the Gd magnetic moments as they are located at $z = 0$. There is no extra constraint for the spin direction of the Mn^{4+} sites as the mirror plane does not pass through those ions. Consequently, six independent Fourier coefficients are needed to describe the modulated Mn^{4+} spins (Table II in the Appendix). Figures 5(a) and 5(c) display the magnetic structure projected on the ab and ac planes. Figure 5(b) shows the nontrivial magnetic domain of the ICM phase with

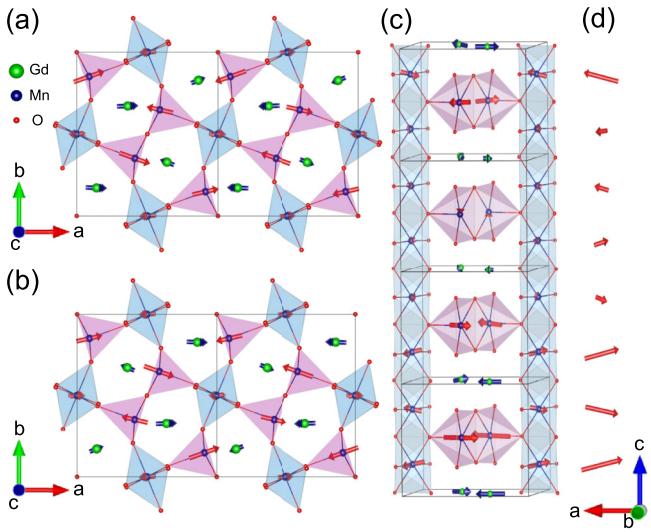

FIG. 5. (a) The ICM magnetic structure of GMO in the *ab* plane at 33.5 K. The dark-blue and red arrows denote the Gd and Mn spins, respectively. (b) The magnetic structure twin with opposite polarization. (c) The magnetic structure projected in the *ac* plane shown with unit cells along the *c* axis. (d) The Mn^{4+} spins projected in the *ac* plane. The moments are scaled by a factor of 2 to highlight the weak modulation along the *c* axis.

opposite polarization. The ICM spin configuration is quite similar to the CM one shown in Fig. 2; the spins mainly reside in the *ab* plane, with small *c*-axis components at all magnetic sites. The small ICM value of q_z also indicates a large periodicity along the *c* axis.

Our bulk measurement does not detect observable electric polarization above 33 K. However, if the exchange striction mechanism is still valid above T_{N2}, one can use Eq. (1) to calculate the polarization. The value averaging from ten stacked layers ($q_z = 0.1$) is finite and about three times smaller than the value at 5 K. Such a value is somewhat inconsistent with the experimental observation (Fig. 1). The sudden change of P in other RMn_2O_5 systems has been extensively discussed [53–55]. For instance, P reduces ~80% below the CM-ICM transition in YMn_2O_5. One main factor for the reduced value is the rotation of the magnetic spins at low T [54]. The Mn^{4+} and Mn^{3+} moments are nearly perpendicular to each other which reduces the dot-product term in Eq. (1). It is also possible that different mechanisms are invoked for distinct magnetic phases; i.e., the spin-current model is needed because of the nonlinearity of cycloidal spin structure, which adversely contributes to the total polarization [55,56]. Simultaneous measurements of the electric polarization and magnetic chirality indeed revealed the polarization in the CM phase is primarily caused by the exchange striction mechanism and becomes DM-interaction driven when the magnetic configuration is ICM [55]. It is important to emphasize that the ICM magnetic structure of $GdMn_2O_5$ is polar, which is consistent with the recent report of a noncentrosymmetric space group in RMn_2O_5 via x-ray and optical second-harmonic generation [57]. The results by Balédent *et al.* indicate that ferroelectricity is already present even at room temperature. In $GdMn_2O_5$, the lack of observable P above T_{N2} strongly indicates that exchange striction is no longer the microscopic mechanism for the polarization. Even if the DM interaction is considered, the polarization is expected to be nearly zero as the refined spin directions are dominantly parallel or antiparallel. Thus, our experimental characterization of the magnetic configuration prompts further theoretical approach to describe the magnetoelectric coupling in this multiferroic family.

In summary, the magnetic structures of multiferroic GMO have been studied by single-crystal neutron diffraction. The CM magnetic structure is nearly collinear and all spins are mostly in the *ab* plane. The magnetic structure reveals that the symmetric exchange striction between the Mn ions is the main driving force for the ferroelectricity. The different T evolution of the ordered Gd^{3+} moment and polarization suggests the magnetoelectric coupling between the $4f$-$3d$ ions is weak and is not responsible for the large polarization of GMO. The ICM magnetic configuration is similar to the CM one, with cycloidal modulation of the moments along the *c* axis. The lack of observable polarization in the ICM phase indicates the exchange striction mechanism does not play a significant role for polarization in that spin configuration.

ORNL is managed by UT-Battelle, LLC under Contract No. DE-AC05-00OR22725 for the U.S. Department of Energy. The U.S. Government retains and the publisher, by accepting the article for publication, acknowledges that the U.S. Government retains a nonexclusive, paid-up, irrevocable, worldwide license to publish or reproduce the published form of this manuscript, or allow others to do so, for U.S. Government purposes. The Department of Energy will provide public access to these results of federally sponsored research in accordance with the DOE Public Access Plan.

We thank J. M. Perez-Mato and L. C. Chapon for stimulating discussion. Research at ORNL was sponsored by the Scientific User Facilities Division, Basic Energy Sciences, U.S. Department of Energy (DOE). J.M.S. acknowledges support from China Scholarship Council. Work at Rutgers University was supported by the DOE under Grant No. DE-FG02-07ER46382. The work in Houston is supported in part by the U.S. Air Force Office of Scientific Research Grant No. FA9550-15-1-0236, the T. L. L. Temple Foundation, the John J. and Rebecca Moores Endowment, and the State of Texas through the Texas Center for Superconductivity at the University of Houston.

APPENDIX: MAGNETIC STRUCTURE REFINEMENTS OF THE CM AND ICM PHASES

The CM magnetic structure of GMO was studied using the four-circle single-crystal diffractometer HB3A at 5 K with incident neutron wavelength of 1.5424 Å. The ICM magnetic structure was studied using the single crystal diffuse scattering spectrometer CORELLI at ORNL. The data were collected for 30 minutes at every orientation with a total time of approximately 35 hours. The raw Bragg intensities were obtained using a 3D ellipsoidal integration method. Data reduction including Lorentz, absorption, TOF spectrum, and detector efficiency corrections were carried out. The refined structural parameters are listed in Tables I and II.

TABLE I. The refined magnetic structure parameters of the CM phases at $T = 5$ and 20 K in GMO. The magnetic Fourier coefficients for each site in the primitive unit cell are along the crystallographic directions. The phase for each site (Φ) is given in units of 2π. The phase of Gd^{3+} is fixed at zero and the refined phases for the other magnetic sites (Φ_i) are close to zero. The error bars are given in parentheses. The reliability coefficient is $R_F = 5.80\%$ at 5 K and $R_F = 6.47\%$ at 20 K. The calculated polarization is $P_b = 47.39c_1 + 25.75c_2$ at 5 K and $P_b = 21.00c_1 + 17.48c_2$ at 20 K, and c_1 and c_2 are the magnetoelectric coupling constants between the Gd^{3+}-Mn^{4+} and Mn^{3+}-Mn^{4+} pairs.

Atom	Position	M_x	M_y	M_z	M_{tot} (μ_B)	M_{phase} (Φ_i)
		$T = 5\,\text{K}$, $q_{\text{CM}} = (0.5, 0, 0)$				
Gd_1^{3+}	0.1388(3),0.1709(4),0	6.66(13)	0.39(16)	0.0	6.67(13)	$\Phi_1 = 0$
Gd_2^{3+}	0.6388(3),0.3291(4),0	−5.97(10)	2.44(21)	0.0	6.45(11)	$\Phi_2 = 0$
Mn^{4+}	0,1/2,0.2558(10)	−2.06(8)	0.82(11)	−0.33(16)	2.24(8)	$\Phi_3 = 0$
Mn_1^{3+}	0.4115(7),0.3523(9),1/2	3.33(13)	−0.43(20)	0.0	3.36(13)	$\Phi_4 = 0$
Mn_2^{3+}	0.5885(7),0.6477(9),1/2	−3.48(14)	0.99(16)	0.0	3.62(14)	$\Phi_5 = 0$
		$T = 20\,\text{K}$, $q_{\text{CM}} = (0.5, 0, 0)$				
Gd_1^{3+}	0.1388(3),0.1709(4),0	3.67(20)	0.02(1)	0.0	3.67(20)	$\Phi_1 = 0$
Gd_2^{3+}	0.6388(3),0.3291(4),0	−3.02(18)	1.70(30)	0.0	3.46(21)	$\Phi_2 = 0$
Mn^{4+}	0,1/2,0.2558(10)	−1.72(11)	0.82(17)	−0.91(33)	2.11(18)	$\Phi_3 = 0$
Mn_1^{3+}	0.4115(7),0.3523(9),1/2	2.88(23)	−0.18(30)	0.0	2.88(23)	$\Phi_4 = 0$
Mn_2^{3+}	0.5885(7),0.6477(9),1/2	−2.71(24)	1.22(25)	0.0	2.96(22)	$\Phi_5 = 0$

TABLE II. The refined magnetic structure parameters in the ICM phases at $T = 33.5$ and 36 K in GMO. The phase of Gd^{3+} is fixed at zero. $R_F = 6.16\%$ at 33.5 K and $R_F = 8.06\%$ at 36 K. If using a similar exchange striction mechanism as in Eq. (1), the calculated polarization is $P_b = 4.61c_1 + 8.24c_2$ at 33.5 K and $P_b = 2.55c_1 + 6.97c_2$ at 36.0 K.

Atom	Position	M_x	M_y	M_z	iM_x	iM_y	iM_z	$M_{\text{phase}}(\Phi_i)$
			$T = 33.5\,\text{K}$, $q_{\text{ICM}} = (0.5, 0, 0.1)$					
Gd_1^{3+}	0.139(1),0.172(1),0	1.88(12)	−0.08(12)	0.0	0.0	0.0	0.02(22)	$\Phi_1 = 0.0$
Gd_2^{3+}	0.639(1),0.328(1),0	−1.23(8)	0.55(18)	0.0	0.0	0.0	−0.14(29)	$\Phi_2 = 0.0$
Mn^{4+}	0,1/2,0.256(2)	−1.46(5)	0.10(10)	0.24(35)	−0.29(19)	−0.12(14)	0.13(13)	$\Phi_3 = 0.0256$
Mn_1^{3+}	0.411(2),0.349(3),1/2	2.73(13)	−0.95(26)	0.0	0.0	0.0	0.05(28)	$\Phi_4 = 0.05(1)$
Mn_2^{3+}	0.589(2),0.651(3),1/2	−2.44(11)	0.50(13)	0.0	0.0	0.0	0.01(28)	$\Phi_5 = 0.05(1)$
			$T = 36.0\,\text{K}$, $q_{\text{ICM}} = (0.5, 0, 0.183)$					
Gd_1^{3+}	0.139(1),0.172(1),0	1.42(11)	0.01(12)	0.0	0.0	0.0	−0.06(23)	$\Phi_1 = 0.0$
Gd_2^{3+}	0.639(1),0.328(1),0	−0.83(6)	0.12(14)	0.0	0.0	0.0	−0.17(29)	$\Phi_2 = 0.0$
Mn^{4+}	0,1/2,0.256(2)	−1.22(5)	0.06(12)	0.54(41)	0.10(18)	−0.05(4)	0.08(12)	$\Phi_3 = 0.0468$
Mn_1^{3+}	0.411(2),0.349(3),0.5	2.24(12)	−0.85(25)	0.0	0.0	0.0	0.03(26)	$\Phi_4 = 0.0915$
Mn_2^{3+}	0.589(2),0.651(3),0.5	−1.99(9)	0.25(9)	0.0	0.0	0.0	0.33(31)	$\Phi_5 = 0.0915$

[1] A. Inomata and K. Kohn, J. Phys.: Condens. Matter **8**, 2673 (1996).

[2] N. Hur, S. Park, P. A. Sharma, J. S. Ahn, S. Guha, and S.-W. Cheong, Nature (London) **429**, 392 (2004).

[3] N. Hur, S. Park, P. A. Sharma, S. Guha, and S. W. Cheong, Phys. Rev. Lett. **93**, 107207 (2004).

[4] D. Higashiyama, S. Miyasaka, and Y. Tokura, Phys. Rev. B **72**, 064421 (2005).

[5] J. W. Kim, S. Y. Haam, Y. S. Oh, S. Park, S. W. Cheong, P. A. Sharma, M. Jaime, N. Harrison, J. H. Han, G. S. Jeon, P. Coleman, and K. H. Kim, Proc. Natl. Acad. Sci. USA **106**, 15573 (2009).

[6] C. Vecchini, L. C. Chapon, P. J. Brown, T. Chatterji, S. Park, S. W. Cheong, and P. G. Radaelli, Phys. Rev. B **77**, 134434 (2008).

[7] J. A. Alonso, M. T. Casais, M. J. Martínez-Lope, J. L. Martínez, and M. T. Fernández-Díaz, J. Phys.: Condens. Matter **9**, 8515 (1997).

[8] L. C. Chapon, G. R. Blake, M. J. Gutmann, S. Park, N. Hur, P. G. Radaelli, and S. W. Cheong, Phys. Rev. Lett. **93**, 177402 (2004).

[9] N. Lee, C. Vecchini, Y. J. Choi, L. C. Chapon, A. Bombardi, P. G. Radaelli, and S. W. Cheong, Phys. Rev. Lett. **110**, 137203 (2013).

[10] G. R. Blake, L. C. Chapon, P. G. Radaelli, S. Park, N. Hur, S. W. Cheong, and J. Rodriguez-Carvajal, Phys. Rev. B **71**, 214402 (2005).

[11] C. R. dela Cruz, F. Yen, B. Lorenz, M. M. Gospodinov, C. W. Chu, W. Ratcliff, J. W. Lynn, S. Park, and S. W. Cheong, Phys. Rev. B **73**, 100406 (2006).

[12] S. W. Cheong and M. Mostovoy, Nat. Mater. **6**, 13 (2007).

[13] J. V. D. Brink and D. I. Khomskii, J. Phys.: Condens. Matter **20**, 434217 (2008).

[14] C. R. dela Cruz, B. Lorenz, Y. Y. Sun, Y. Wang, S. Park, S. W. Cheong, M. M. Gospodinov, and C. W. Chu, Phys. Rev. B **76**, 174106 (2007).

[15] Z. Y. Zhao, M. F. Liu, X. Li, L. Lin, Z. B. Yan, S. Dong, and J. M. Liu, Sci. Rep. **4**, 3984 (2014).

[16] B. C. Chakoumakos, H. Cao, F. Ye, A. D. Stoica, M. Popovici, M. Sundaram, W. Zhou, J. S. Hicks, G. W. Lynn, and R. A. Riedel, J. Appl. Crystallogr. **44**, 655 (2011).

[17] F. Ye, Y. Liu, R. Whitfield, R. Osborn, and S. Rosenkranz, J. Appl. Crystallogr. **51**, 315 (2018).

[18] J. Koo, C. Song, S. Ji, J. S. Lee, J. Park, T. H. Jang, C. H. Yang, J. H. Park, Y. H. Jeong, K. B. Lee, T. Y. Koo, Y. J. Park, J. Y. Kim, D. Wermeille, A. I. Goldman, G. Srajer, S. Park, and S. W. Cheong, Phys. Rev. Lett. **99**, 197601 (2007).

[19] S. Chattopadhyay, S. Petit, E. Ressouche, S. Raymond, V. Baledent, G. Yahia, W. Peng, J. Robert, M. B. Lepetit, M. Greenblatt, and P. Foury-Leylekian, Sci. Rep. **7**, 14506 (2017).

[20] K. Momma and F. Izumi, J. Appl. Crystallogr. **44**, 1272 (2011).

[21] G. Yahia, F. Damay, S. Chattopadhyay, V. Baledent, W. Peng, S. W. Kim, M. Greenblatt, M. B. Lepetit, and P. Foury-Leylekian, Phys. Rev. B **97**, 085128 (2018).

[22] M. I. Aroyo, J. M. Perez-Mato, C. Capillas, E. Kroumova, S. Ivantchev, G. Madariaga, A. Kirov, and H. Wondratschek, Z. Kristallogr. - Cryst. Mater. **221**, 15 (2006).

[23] M. I. Aroyo, A. Kirov, C. Capillas, J. M. Perez-Mato, and H. Wondratschek, Acta Crystallogr., Sect. A: Found. Adv. **62**, 115 (2006).

[24] M. I. Aroyo, J. M. Perez-Mato, D. Orobengoa, E. Tasci, G. de la Flor, and A. Kirov, Bulg. Chem. Commun. **43**, 183 (2011).

[25] J. Perez-Mato, S. Gallego, E. Tasci, L. Elcoro, G. D. L. Flor, and M. Aroyo, Annu. Rev. Mater. Res. **45**, 217 (2015).

[26] J. Rodriguez-Carvajal, Physica B (Amsterdam, Neth.) **192**, 55 (1993).

[27] I. D. Brown and D. Altermatt, Acta Crystallogr., Sect. B: Struct. Sci., Cryst. Eng. Mater. **41**, 244 (1985).

[28] P. P. Gardner, C. Wilkinson, J. B. Forsyth, and B. M. Wanklyn, J. Phys. C **21**, 5653 (1988).

[29] P. G. Radaelli and L. C. Chapon, J. Phys.: Condens. Matter **20**, 434213 (2008).

[30] H. Katsura, N. Nagaosa, and A. V. Balatsky, Phys. Rev. Lett. **95**, 057205 (2005).

[31] G. Lawes, A. B. Harris, T. Kimura, N. Rogado, R. J. Cava, A. Aharony, O. Entin-Wohlman, T. Yildrim, M. Kenzelmann, C. Broholm, and A. P. Ramirez, Phys. Rev. Lett. **95**, 087205 (2005).

[32] Y. Yamasaki, H. Sagayama, T. Goto, M. Matsuura, K. Hirota, T. Arima, and Y. Tokura, Phys. Rev. Lett. **98**, 147204 (2007).

[33] S. C. Abrahams and J. L. Bernstein, J. Chem. Phys. **46**, 3776 (1967).

[34] C. R. dela Cruz, B. Lorenz, W. Ratcliff, J. Lynn, M. M. Gospodinov, and C. W. Chu, Physica B (Amsterdam, Neth.) **403**, 1359 (2008).

[35] I. Kagomiya, K. Kohn, and T. Uchiyama, Ferroelectrics **280**, 131 (2002).

[36] M. Tachibana, K. Akiyama, H. Kawaji, and T. Atake, Phys. Rev. B **72**, 224425 (2005).

[37] B. K. Khannanov, E. I. Golovenchits, and V. A. Sanina, J. Phys.: Conf. Ser. **572**, 012046 (2014).

[38] N. Poudel, M. Gooch, B. Lorenz, C. W. Chu, J. W. Kim, and S. W. Cheong, Phys. Rev. B **92**, 144430 (2015).

[39] L. H. Yin, D. H. Jang, C. B. Park, K. W. Shin, and K. H. Kim, J. Appl. Phys. **119**, 104101 (2016).

[40] S. H. Bukhari, T. Kain, M. Schiebl, A. Shuvaev, A. Pimenov, A. M. Kuzmenko, X. Wang, S. W. Cheong, J. Ahmad, and A. Pimenov, Phys. Rev. B **94**, 174446 (2016).

[41] Y. Ishii, S. Horio, M. Mitarashi, T. Sakakura, M. Fukunaga, Y. Noda, T. Honda, H. Nakao, Y. Murakami, and H. Kimura, Phys. Rev. B **93**, 064415 (2016).

[42] T. Fujita and K. Kohn, Ferroelectrics **219**, 155 (1998).

[43] I. Kagomiya, S. Matsumoto, K. Kohn, Y. Fukuda, T. Shoubu, H. Kimura, Y. Noda, and N. Ikeda, Ferroelectrics **286**, 167 (2003).

[44] R. P. Chaudhury, C. R. dela Cruz, B. Lorenz, Y. Sun, C.-W. Chu, S. Park, and S.-W. Cheong, Phys. Rev. B **77**, 220104(R) (2008).

[45] M. Fukunaga, K. Nishihata, H. Kimura, Y. Noda, and K. Kohn, J. Phys. Soc. Jpn. **76**, 074710 (2007).

[46] B. Roessli, P. Fischer, P. J. Brown, M. Janoschek, D. Sheptyakov, S. N. Gvasaliya, B. Ouladdiaf, O. Zaharko, G. Eu, and V. Sanina, J. Phys.: Condens. Matter **20**, 485216 (2008).

[47] Y. Noda, H. Kimura, Y. Kamada, T. Osawa, Y. Fukuda, Y. Ishikawa, S. Kobayashi, Y. Wakabayashi, H. Sawa, N. Ikeda, and K. Kohn, Physica B (Amsterdam, Neth.) **385-386**, 119 (2006).

[48] J. B. Goodenough, Phys. Rev. **100**, 564 (1955).

[49] There is a relatively large variation in measured polarization from different groups for $GdMn_2O_5$. We used the averaged polarization at 5 K to deduce the magnetoelectric coupling constant $c_2 = 103.3\ \mu C/m^2$. The value of c_2 is further used to calculate the polarization of the other RMn_2O_5 materials.

[50] L. C. Chapon (private communication).

[51] J. M. Perez-Mato, J. L. Ribeiro, V. Petricek, and M. I. Aroyo, J. Phys.: Condens. Matter **24**, 163201 (2012).

[52] V. Petříček, M. Dušek, and L. Palatinus, Z. Kristallogr. - Cryst. Mater. **229**, 345 (2014).

[53] J. H. Kim, S. H. Lee, S. I. Park, M. Kenzelmann, A. B. Harris, J. Schefer, J. H. Chung, C. F. Majkrzak, M. Takeda, S. Wakimoto, S. Y. Park, S. W. Cheong, M. Matsuda, H. Kimura, Y. Noda, and K. Kakurai, Phys. Rev. B **78**, 245115 (2008).

[54] P. G. Radaelli, C. Vecchini, L. C. Chapon, P. J. Brown, S. Park, and S. W. Cheong, Phys. Rev. B **79**, 020404 (2009).

[55] S. Wakimoto, H. Kimura, Y. Sakamoto, M. Fukunaga, Y. Noda, M. Takeda, and K. Kakurai, Phys. Rev. B **88**, 140403 (2013).

[56] Y. Tokura, S. Seki, and N. Nagaosa, Rep. Prog. Phys. **77**, 076501 (2014).

[57] V. Balédent, S. Chattopadhyay, P. Fertey, M. B. Lepetit, M. Greenblatt, B. Wanklyn, F. O. Saouma, J. I. Jang, and P. Foury-Leylekian, Phys. Rev. Lett. **114**, 117601 (2015).